6900–6916 *Nucleic Acids Research, 2019, Vol. 47, No. 13* *Published online 5 June 2019*
doi: 10.1093/nar/gkz500

mRNA levels can be reduced by antisense oligonucleotides via no-go decay pathway

Xue-hai Liang*, Joshua G. Nichols, Chih-Wei Hsu, Timothy A. Vickers and Stanley T. Crooke

Department of Core Antisense Research, Ionis Pharmaceutics, Inc., 2855 Gazelle Court, Carlsbad, CA 92010, USA

Received February 05, 2019; Revised May 24, 2019; Editorial Decision May 27, 2019; Accepted June 01, 2019

ABSTRACT

Antisense technology can reduce gene expression via the RNase H1 or RISC pathways and can increase gene expression through modulation of splicing or translation. Here, we demonstrate that antisense oligonucleotides (ASOs) can reduce mRNA levels by acting through the no-go decay pathway. Phosphorothioate ASOs fully modified with 2′-*O*-methoxyethyl decreased mRNA levels when targeted to coding regions of mRNAs in a translation-dependent, RNase H1-independent manner. The ASOs that activated this decay pathway hybridized near the 3′ end of the coding regions. Although some ASOs induced nonsense-mediated decay, others reduced mRNA levels through the no-go decay pathway, since depletion of PELO/HBS1L, proteins required for no-go decay pathway activity, decreased the activities of these ASOs. ASO length and chemical modification influenced the efficacy of these reagents. This non-gapmer ASO-induced mRNA reduction was observed for different transcripts and in different cell lines. Thus, our study identifies a new mechanism by which mRNAs can be degraded using ASOs, adding a new antisense approach to modulation of gene expression. It also helps explain why some fully modified ASOs cause RNA target to be reduced despite being unable to serve as substrates for RNase H1.

INTRODUCTION

Antisense technology, in which antisense oligonucleotides (ASOs) hybridize with target RNAs to result in specificity, can modulate gene expression via different mechanisms (1–4). Enzyme-mediated reduction of target RNAs involves RNase H1- or RNA induced silencing complex (RISC)-dependent mechanisms (1,5). Non-RNase-mediated mechanisms have also been developed. Though RNase H1-dependent ASOs are designed to contain deoxyribonucleotides in the center flanked by modified nucleotides at both ends, known as gapmers, non-gapmer ASOs that do not trigger RNase H1 cleavage can modulate splicing to influence the mRNA isoforms produced (6,7). The nonsense-mediated decay (NMD) of mRNAs can be regulated by ASOs that target the binding sites of the exon-exon junction complex, by using ASOs to reduce levels of NMD factors to increase mRNA levels (8,9), or by using ASOs to induce NMD via an influence on alterative splicing (10). These approaches highlight the versatility of antisense technology. ASO technology is used in research and multiple antisense drugs have now received approval for clinical use (11,12).

ASO drugs are chemically modified to enhance stability, delivery, and pharmacological properties (13–17). Modifications include but are not limited to the backbone phosphorothioate (PS) modification and ribose modifications such as 2′-*O*-methyl (2′-OMe), 2′-*O*-methoxyethyl (2′-MOE), constrained ethyl (cEt), locked nucleic acid (LNA), and 2′-fluoro (2′-F), which significantly affect the physicochemical properties of ASOs (15,18,19). For example, the PS linkage reduces the melting temperature (T_m) of the duplex between ASO and target RNA but enhances ASO-protein interactions and ASO stability in biological systems (13,15,20). The commonly used 2′-modifications enhance ASO stability and increase T_m to varying extents: 0.5–1°C per modification for 2′-OMe and 2′-MOE, 2–5°C per modification for cEt, LNA and 2′-F (21–23). In addition, 2′-modifications also influence the protein binding properties of ASOs. cEt, LNA and 2′-F-modified ASOs bind more proteins more avidly than 2′-MOE modified ASOs (13,24–29). These features provide opportunities to design ASOs with optimal performance.

Splicing modulating ASOs act in the nucleus, whereas RNase H1-dependent ASOs act in both the nucleus and the cytoplasm to trigger target RNA degradation (30,31). ASOs that act as steric blockers to reduce protein levels by inhibiting translation or to enhance translation through targeting upstream open reading frames and translation inhibitory elements act in the cytoplasm (32–35). Activi-

*To whom correspondence should be addressed. Tel: +1 760 603 3816; Fax: +1 760 603 2600; Email: Lliang@ionisph.com

ties of certain ASOs that operate through an RNase H1-dependent mechanism are influenced by translation. For instance, ASO activity can be reduced by translation when the ASO targets the coding region of an efficiently translated mRNA (36). This observation raised the possibility that ASOs that interact with mRNAs to modulate translation may affect the fate of mRNAs by triggering mRNA degradation through translation-mediated decay pathways.

In addition to normal mRNA decay pathways that can be mediated by poly(A) shortening and decapping (37–42), other decay pathways also exist to ensure mRNA and protein quality. These include the nonsense-mediated decay (NMD), non-stop decay (NSD), and no-go decay (NGD) pathways, and perhaps other pathways as well (43–49). NMD is triggered by the presence of premature termination codons and requires a set of proteins including UPF1, an RNA helicase, and SMG6, a mammalian-specific protein with endonuclease activity (43,44). NSD is induced when ribosomes are stalled at the 3′ end of mRNAs lacking a termination codon, and Ski7 and exosomes are required for degradation of the mRNAs as demonstrated in yeast (50).

NGD was initially identified in yeast and has now been shown to be active in insects, plants, and mammals (48,51–53). NGD is translation dependent and is triggered by obstacles that impede ribosome movement along the mRNA. mRNA structure or the presence of clustered inhibitory and rare codons can cause ribosome stalling and lead to mRNA degradation (49). The collision of multiple ribosomes on the mRNA template appears to be critical for the NGD process. Therefore the stall site must be located at a distance downstream from the start codon (>105 nt) such that sufficient numbers of ribosomes can be bound (54). Endonuclease cleavage sites are located upstream of the stall site, likely between the stalled ribosomes (54,55). The 5′ and 3′ cleaved fragments are processed by the 3′→5′ exonuclease activity of the exosome and by the 5′→3′ exonuclease Xrn1, respectively (48). The endonuclease responsible for NGD cleavage has not been identified. PELO (the human counterpart of the yeast Dom34) and HBS1L proteins are required for NGD; these two factors likely interact with the stalled ribosomes (48,51,56). Dom34 contains a potential endonuclease domain, but this domain is not required for NGD-mediated mRNA cleavage, as demonstrated by mutational analyses (51), and the endonuclease activity was also not supported by structural studies (56–58).

Previously, it was demonstrated that some ASOs with activity not dependent on RNase H1 could reduce mRNA levels via unknown mechanisms (59). Here we demonstrate that non-gapmer ASOs can influence gene expression by inducing mRNA degradation through the NGD pathway. We found that some uniformly modified PS-MOE ASOs significantly reduced levels of *nucleolin* (*NCL*) mRNA when targeted to the coding region, especially to regions near the 3′ end of the coding region. Some ASOs were found to trigger the NMD pathway, and others the NGD pathway. The activities of NGD-mediating ASOs are dependent on translation and PELO/HBS1L proteins, but not on NMD pathway proteins UPF1/SMG6. Together, our results indicate that appropriately designed ASOs can reduce mRNA levels via the NGD pathway, providing an additional antisense approach to modulate gene expression.

MATERIALS AND METHODS

Cell culture and transfection of ASOs, siRNAs, and plasmids

HeLa, HEK293, Hep3B and bEND.3 cells were cultured in Dulbecco's modified Eagle's medium (DMEM) supplemented with 10% fetal bovine serum (FBS), 0.1 μg/ml streptomycin and 100 units/ml penicillin in a 37°C incubator with 5% CO_2. Cells were seeded at approximately 50% confluency 16 h before transfection. For ASO activity assays, cells grown in 96-well plates were transfected for 5 h with ASOs using 4 μg/ml Lipofectamine 2000 in Opti-MEM medium (Life Technologies) based on manufacturer's instructions. Medium was then replaced with prewarmed complete DMEM medium, and cells were incubated for 16 h before RNA preparation.

Cells were transfected with siRNA using 5 μg/ml Lipofectamine RNAiMax (Life Technologies) based on manufacturer's procedure with a final siRNA concentration of 5 nM. Medium was replaced with fresh medium 8 h after siRNA transfection. After 36 h, cells were re-seeded in 96-well plates at ∼70% confluency, incubated overnight, and transfected with ASOs. Alternatively, siRNA-treated cells were collected 72 h after transfection and cell lysate was prepared for western analysis.

For cycloheximide (CHX) treatment, HeLa cells grown in 96-well plates were treated with 100 μg/ml CHX alone, transfected with 75 nM ASO alone, or were treated with both ASO and CHX. Cells were collected at different times after treatment, and total RNA was prepared. For plasmid transfection, 1.5 μg plasmid DNA was transfected into HeLa cells grown in a 10-cm dish using Effectene (Qiagen) based on the manufacturer's instructions. After 24 h, cells were re-seeded in 96-well plates, incubated for 16 h, and transfected with ASOs. ASO and siRNA sequences are listed in Supplementary Data.

RNA preparation and qRT-PCR analysis

Total RNA was prepared from cells using RNeasy mini kit (Qiagen), based on manufacturer's procedure. Quantitative real-time RT-PCR (qRT-PCR) analyses were conducted as described previously (26). Briefly, qRT-PCR was performed in triplicate using StepOne Real-Time PCR system. Primer and probe sequences are listed in Supplementary Data. One-step qRT-PCR was performed using an AgPathID One-step RT-PCR kit (Applied Biosystems) using the following program: 48°C for 10 min, 94°C for 10 min, and 40 cycles of 20 s each at 94°C and 60°C. The qRT-PCR results were quantified using StepOne Software V2.3. Tested RNA levels in each reaction were normalized to total RNA levels measured using SYBR Green (Life Technologies); average values are reported. For quantification of RNAs prepared from different gradient fractions, the relative mRNA level in each fraction was calculated as percentage of the RNA in the fraction relative to the sum of the mRNA quantities in all fractions. The relative *NCL* mRNA levels in each fraction were then normalized to the relative mRNA levels of *ANXA2* in the fraction. Statistical analysis was performed using Prism with either *t*-test or *F*-test for curve comparison based on non-linear regression (dose-response curves) for XY analyses using the equation

'log(agonist) vs. normalized response – variable slop'. The Y axis (relative level) was used as the normalized response. All the qRT-PCR experiments were performed at least three times, and representative results are shown.

Reverse transcription and PCR

To detect splicing isoforms, total RNA was prepared from ASO-treated cells grown in six-well dishes using RNeasy columns, and 20 ng total RNA was used per reaction. Reverse transcription was performed at 45°C for 30 min, and the PCR reaction was performed with following program: 94°C for 10 min, 28 cycles (Figure 2C) or 35 cycles (Figure 2D) of 45 s each at 94°C and 53°C. Primer sequences are listed in Supplementary Data. The PCR products were analyzed on an 1% agarose gel.

Sucrose gradient fractionation and polysome profiling

Polysome analyses were performed as described previously (33). Briefly, ∼5 × 10^6 HeLa cells were transfected with 70 nM ASOs for 16 or 24 h, and treated for an additional 15 min at 37°C with 100 μg/ml CHX. Cells were washed three times with ice-cold 1× PBS buffer containing 100 μg/ml CHX and pelleted. The cell pellet was washed and resuspended in 600 μl lysis buffer (20 mM Tris pH 7.5, 5 mM $MgCl_2$, 100 mM KCl, 100 μg/ml CHX, 2 mM DTT, 1000 unit/ml of RNaseOut (ThermoFisher)). After incubation on ice for 10 min, cells were lysed by addition of 37 μl of 10% Triton X-100 and 37 μl of 10% sodium deoxycholate, followed by incubation on ice for 5 min. Cell lysates were then prepared by centrifugation at 4°C for 10 min at 12 000 rpm, and 200 μl lysate was loaded onto an 11 ml, 7–47% sucrose gradient. After centrifugation at 35 000 rpm for 2 h at 4°C using a SW41 rotor, 400-μl fractions were collected from top to bottom. RNA was prepared from 200 μl of each fraction using the RNeasy kit (Qiagen), and RNA levels were analyzed by qRT-PCR using primers and probes listed in Supplementary Data. The relative levels of *NCL* mRNA in each fraction was calculated as the percentage of *NCL* mRNA in that fraction, considering the sum of *NCL* mRNA levels in all fractions as 100%. The calculated *NCL* mRNA levels in each fraction were further normalized to the ratios of the relative percentage of an untargeted mRNA, *ANXA2*, in the same fractions between ASO treated and untreated samples.

Western analysis

Cells were collected using trypsin and washed with 1× PBS. Cell lysates were prepared using RIPA buffer (ThermoFisher). Samples were centrifuged at 12 000 × g for 10 min at 4°C. Proteins (30 μg/lane) were separated by 4–12% SDS-PAGE and transferred to membranes. Target proteins were detected with antibodies listed in Supplementary Data, and visualized using enhanced chemiluminescence.

T_m analysis

The thermal stabilities (T_m) of the duplexes formed by the oligonucleotides and a complementary RNA were analyzed by measuring the UV absorbance versus temperature curves as described previously (60). Each sample contained 100 mM NaCl, 10 mM sodium phosphate (pH 7.0), 0.1 mM EDTA, 4 μM oligonucleotide and 4 μM complementary RNA. The sequences of ASOs and complementary RNAs are listed in Supplementary Data.

Affinity selection

Affinity selection using biotinylated ASO 386652 was performed essentially as described previously (26). Proteins were eluted using PS-MOE ASO 1199616, or PS/MOE ASOs containing the cEt modification 1215826 or 1215829. Eluted proteins were separated on 4–12% SDS-PAGE gel, and PELO or HBS1L proteins were detected by immunoblotting.

Bioluminescence resonance energy transfer (BRET) binding assay

HBS1L NanoLuc (Nluc) fusion protein construction, expression, and purification were performed essentially as described (61). Briefly, full-length human *HBS1L* (NM_006620) was amplified by PCR from the cDNA clone (Origene RC208125). The forward PCR primer (5′-gctagc AGCCACCATGGCCCGGCATCGGAATG-3′) was complimentary to the *HBS1L* sequence around the AUG start codon and preceded by a Kozak sequence. The forward primer included a NheI site. The reverse primer (5′- GGTGTTGTCACTGAG ATAAAAGAAgactcgag) was complementary to the *HBS1L* sequence upstream of the stop codon, and contained an XhoI site. The PCR amplified product was ligated into NheI and XhoI sites of the NanoLuc expression vector pFC32K Nluc CMV-Neo (Promega) to create an in-frame C-terminal NLuc fusion. A 6X HIS-tag (encoded by 5′-CAT CAT CAT CAC CAC CAC-3′) was inserted downstream of the NLuc cassette by site-directed mutagenesis using a Q5 Site-Directed Mutagenesis Kit (New England BioLabs) according to the manufacturer's protocol.

The HBS1L-NLuc fusion protein was expressed by transfecting the plasmids into 6 × 10^5 HEK293 cells using Effectene transfection reagent according to the manufacturer's protocol (Qiagen). Following a 24-h incubation, cells were removed from the plate by trypsinization, washed with PBS, and resuspended in 250 μl Pierce IP Lysis Buffer (Thermo Scientific). The lysate was incubated 30 min at 4°C while rotating, then debris pelleted by centrifugation at 15 000 rpm for 5 min. The fusion protein was purified by adding 20 μl HisPur Ni-NTA Magnetic Beads (Thermo Scientific) and 10 mM imidazole then incubating at 4°C for 2 h. The beads were then washed four times with 10 mM imidazole and 0.01% Tween-20 in PBS. The HBS1L-NLuc fusion protein was eluted from the beads in 100 μl 200 mM imidazole in PBS, followed by dilution with 200 μl IP buffer.

BRET assays were performed in white 96-well plates as previously described (20). In brief, 50 nM Alexa-594 linked MOE gapmer ASO 766634 was incubated with 1–10 000 nM ASO of interest for 15 min at room temperature in 100 mM NaCl, 20 mM Tris–HCl, pH 7.5, 1 mM EDTA, 0.1% NP-40 with 10^6 relative light units (RLU) per well of

Ni-NTA-purified NLuc fusion protein. Following the incubation, NanoGlo substrate (Promega) was added at 0.1 μl/well. Readings were performed for 0.3 s using a Glomax Discover system using 450-nm/8-nm band pass for the donor filter and 600-nm long pass for the acceptor filter. BRET was calculated as the ratio of the emission at 600 nm to that at 450 nm (fluorescent excitation emission/RLU).

RESULTS

Uniform PS-MOE ASOs can reduce the level of *NCL* mRNA in different cells and species

To understand the potential mechanisms of mRNA reduction by ASOs that cannot initiate RNase H1 cleavage of RNA, 80 ASOs fully modified with PS and 2′-MOE (PS-MOE ASOs) were synthesized that target different positions of *NCL* mature mRNA, including the 5′ UTR, coding region, and 3′ UTR sequences. The ASO sequences were filtered to exclude certain features, such as CpG dinucleotide, G-clusters, and potential immune motifs. These ASOs cannot trigger RNase H1 cleavage of the target RNAs, as RNase H1 requires DNA/RNA heteroduplex formation (62,63).

HeLa cells were transfected with ASOs for 18 h, and the levels of *NCL* mRNA were determined by qRT-PCR (Figure 1A). As expected, most ASOs did not substantially reduce the levels of *NCL* mRNA; however, certain ASOs dramatically decreased the mRNA levels compared to levels in mock treated control cells. This experiment was repeated three times, with different primer probe sets for qRT-PCR, and similar results were obtained (data not shown), with the exception of ASO 1199558, which did not reduce the mRNA level in other experiments (Supplementary Figure S1A). The ASOs that triggered substantial mRNA reduction mainly targeted sequences toward the 3′ end of the coding region. The most 5′ site bound by an active ASO (ASO 1199568) was 162 nucleotides (nt) downstream from the AUG start codon. No substantial mRNA reduction was induced by ASOs targeting 5′ or 3′ UTR sequences.

To further confirm this observation and to determine the kinetics of ASO action, detailed dose-response studies were performed for seven uniform PS-MOE ASOs. HeLa cells were transfected with these ASOs at different concentrations, and the levels of *NCL* mRNA were quantified using qRT-PCR at 5 and 24 hours after transfection (Figure 1B and C). A 5–10-5 gapmer PS-ASO 110080, which reduces mRNA levels via RNase H1 cleavage (30), was also tested. Although the PS-MOE ASOs reduced *NCL* mRNA levels by more than 80% at 24 hours after transfection compared to the control-treated cells (Figure 1C), only approximately 40% reduction was achieved at 5 hours after transfection at highest ASO concentration (Figure 1B). This is in contrast to the RNase H1-dependent gapmer ASO 110080, which reduced mRNA levels much more rapidly (>95% reduction for 5 h at the highest concentration tested).

The activities of the uniform PS-MOE ASOs appear to be weaker than that of gapmer ASOs targeting the same sites (Supplementary Figure S1B). However, more than a decade of research has resulted in the gapmer ASO design optimized to serve as substrates for RNase H1, so future investigation on these uniform PS-MOE ASOs could enhance activity. Nevertheless, these observations together suggest that the mechanism that underlies the reduction of the mRNA levels by the uniform PS-MOE ASOs occurs more slowly than RNase H1 cleavage. Consistent with the reduced level of *NCL* mRNA, the NCL protein level was also decreased by the PS-MOE ASO 1199600 (Figure 1D). In addition, comparable protein reduction was achieved by ASO 1199600 and the gapmer ASO 110093 targeting the same site (Supplementary Figure S1C), although the gapmer ASO is more active than ASO 1199600 in reducing the mRNA levels (Supplementary Figure S1B).

The reduction of *NCL* mRNA by uniformly modified PS-MOE ASOs was not due to unexpected effects of transfection, as the majority of tested ASOs transfected in the same way did not reduce the mRNA level (Figure 1A). In addition, we did not observe substantial reduction of pre-mRNA at either 5 or 24 hours after transfection (Supplementary Figure S2A and B), suggesting that the reduction in mRNA levels did not result from impaired transcription. Further, the levels of an untargeted transcript, *Drosha* mRNA, were not substantially affected by treatment of cells with PS-MOE ASOs targeting *NCL* mRNA (Supplementary Figure S2C). These results suggest that PS-MOE ASOs can specifically reduce the level of targeted mRNA in an RNA binding position-dependent manner. *NCL* mRNA levels in HEK293 and Hep3B cells (Supplementary Figure S3A and B, respectively) and in mouse bEND.3 cells (Supplementary Figure S3C and D) were also reduced by select PS-MOE ASOs, although with different potencies. Together, these results indicate that uniform PS-MOE ASOs can reduce mRNA levels in different cell types.

Some PS-MOE ASOs alter splicing patterns yet other ASOs do not

It has been demonstrated previously that uniform PS-MOE ASOs can act on pre-mRNA and affect splicing, leading to alternatively spliced transcripts that can be subjected to NMD (10). To determine whether the uniform PS-MOE ASOs targeted to *NCL* affected splicing, 14 ASOs that reduced *NCL* mRNA levels to different extents were transfected into HeLa cells, and the levels of mature mRNA and pre-mRNA were evaluated at 18 hours after transfection using primer probe sets specific to mature mRNA or pre-mRNA. The level of *NCL* mRNA was reduced to different extents by these ASOs (Figure 2A). No substantial increase in pre-mRNA levels was detected by the qRT-PCR upon transfection of these ASOs with the exceptions of ASOs 1199578 and 1199607, which increased pre-mRNA levels to about 275% and 150% of levels in control-treated cells, respectively (Figure 2B). Similar changes in the level of the pre-mRNA were observed using a different primer probe set specific to a different region of the *NCL* pre-mRNA (Figure 2C). These results indicate that certain PS-MOE ASOs impaired splicing.

Next, we sought to determine whether ASO treatment triggers alternative splicing of exons adjacent to the ASO target sites. Primers for reverse transcription and PCR were designed that span exons 2–6 (P1), exons 6–9 (P2), and exons 9–13 (P3), *NCL* mRNA regions targeted by different ASOs (Figure 2D, upper panel). Strand-specific reverse

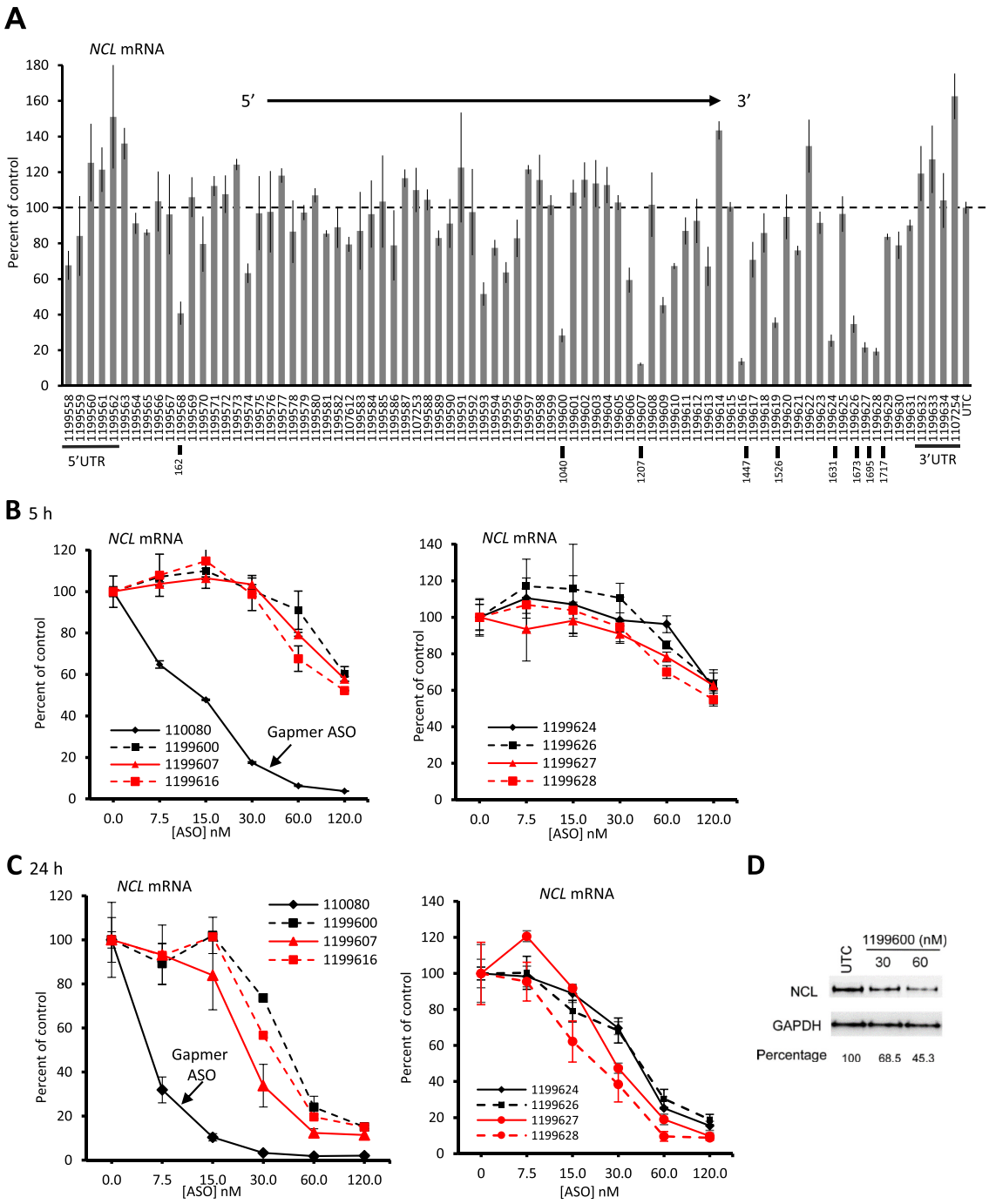

Figure 1. ASOs uniformly modified with PS and 2′-MOE can reduce the levels of *NCL* mRNA. (**A**) qRT-PCR quantification of levels of *NCL* mRNA in HeLa cells at 24 h after transfection with 120 nM ASO. The ID numbers of ASOs are listed on the X-axis in order of hybridization in a 5′ to 3′ direction to *NCL* mRNA. The positions of ASO target sites relative to the AUG start codon are given for selected ASOs that showed substantial activity (the small numbers below the ASO numbers). Percent of control: mRNA levels in each sample relative to that in mock transfected control cells (UTC). (**B**) qRT-PCR quantification of the levels of *NCL* mRNA in HeLa cells 5 h after transfection with ASOs. (**C**) qRT-PCR quantification of the levels of *NCL* mRNA in HeLa cells 24 h after transfection with ASOs. **D**) Western analyses of NCL protein in HeLa cells 48 h after transfection with ASO 1199600. The relative NCL protein level quantified using ImageJ and normalized to GAPDH is shown below the lanes. Error bars in all panels are standard deviations from three independent experiments.

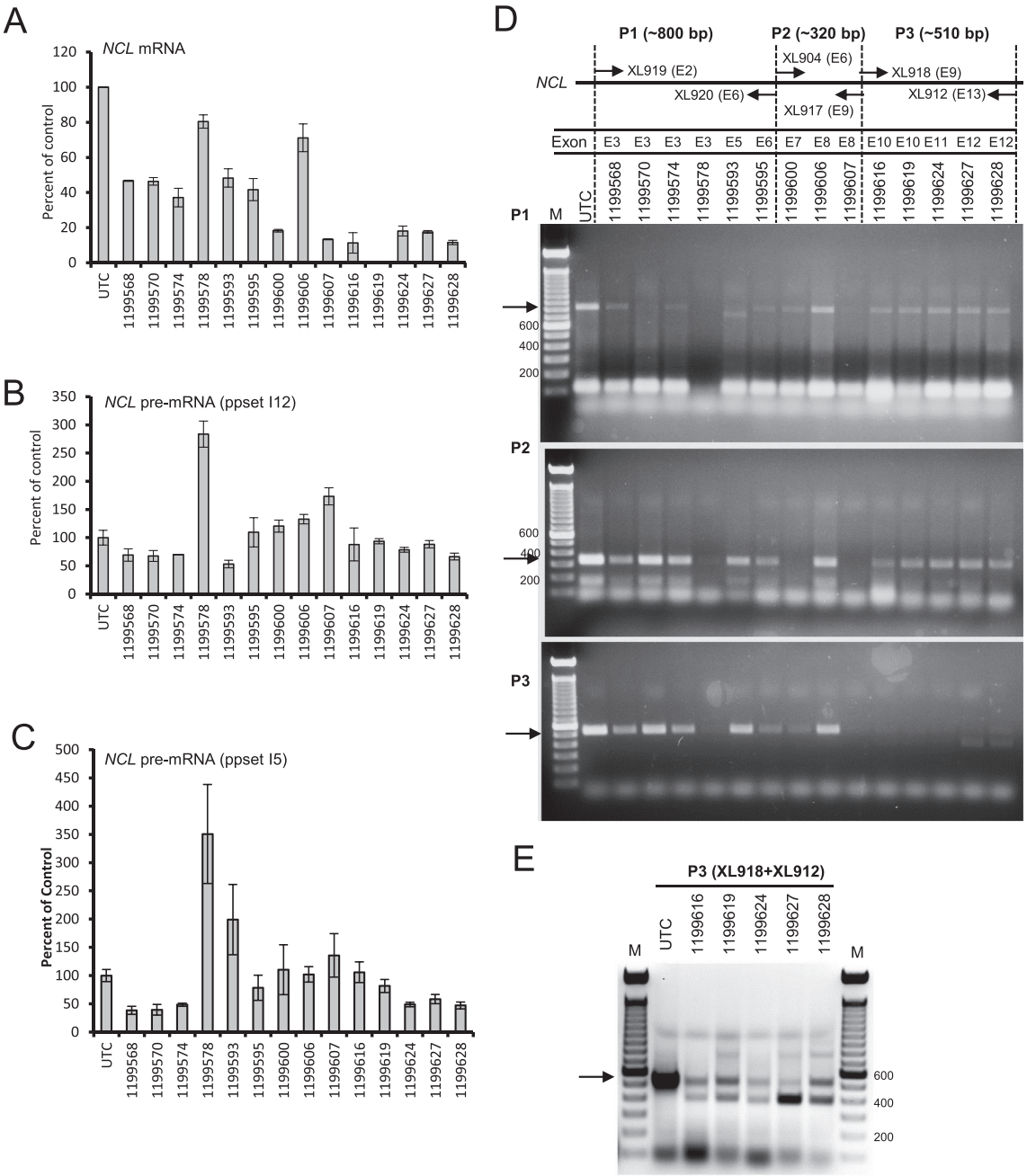

Figure 2. Some PS-MOE ASOs affect pre-mRNA splicing whereas others do not. (**A**) qRT-PCR quantification of the levels of *NCL* mature mRNA in HeLa cells 18 h after transfection with 60 nM ASO. (**B**) qRT-PCR quantification of *NCL* pre-mRNA in the same RNA samples as described in panel A, using a prime probe set spanning intron 12/exon 12 region. (**C**) qRT-PCR quantification of *NCL* pre-mRNA as described above, using a different primer probe set spanning intron 5/exon 6 region. (**D**) Ethidium bromide staining of reverse transcription-PCR products separated on 1% agarose gels. ASOs are listed above the lanes, and expected PCR products are indicated by arrows. PCR primers and their relative positions along the *NCL* mRNA are shown. The exon locations targeted by the ASOs are indicated. Reverse transcription-PCR was performed using primers P1 (upper panel), P2 (middle panel), or P3 (lower panel). M, 100 bp DNA ladder. (**E**) Reverse transcription-PCR analysis of *NCL* mRNA in ASO-treated samples using primers P3 as described in panel C but with more PCR cycles.

transcription was performed to synthesize cDNA and PCR was then conducted to determine the size of the spliced mRNA (Figure 2D, lower panel). No change in the size of the PCR products was observed for any ASO-treated samples when using primer sets specific to mRNA regions outside the ASO-targeted region, further suggesting that global splicing was not impaired by the PS-MOE ASOs.

However, an additional PCR product was detected upon treatment with certain ASOs (ASOs 1199616–1199628) targeting the 3′ region of the coding sequence (Figure 2E). The size of the PCR product in control cells was about 510 base pairs (bp), as expected, whereas a product of about 400 bp was also observed in samples treated with these ASOs. The 400-bp PCR product is the size expected if either exon 10 (∼120 nt) or exon 11 (∼130 nt) were skipped. Sequencing analyses of the PCR products confirmed that ASO 1199616 (targeting exon 10) and 1199624 (targeting exon 11) caused skipping of exon 10 and of exon 11, respectively; ASOs 1199627 and 1199628 that target exon 12 led to skipping of this exon. There are premature termination codons in each of these exon-skipped transcripts (data not shown). Thus, some of the PS-MOE ASOs targeting exon regions of *NCL* did alter pre-mRNA splicing, as reported previously in a study of ASOs targeting *SMN2* (6). No alternatively spliced products were detected for other ASOs, such as ASOs 1199595, 1199600 and 1199606, that reduce levels of *NCL* mature mRNA (Figure 2D). These observations suggest that PS-MOE ASOs targeting the coding region may reduce mRNA levels through a mechanism that does not involve altered splicing.

Certain PS-MOE ASOs reduce *NCL* mRNA levels via the NGD or NMD pathways

Although ASO-triggered alternative splicing could potentially lead to NMD, it is possible that other ASOs that did not alter splicing may induce decay through other pathways. The NGD pathway is known to be triggered by ribosome stalling on mRNA (49). ASOs base paired with certain positions in the mRNA may generate obstructions that hinder ribosome scanning, leading to ribosome stalling. This possibility is supported by the observations that active ASOs were found at positions at least 160 nt downstream from the start codon, but no active ASO hybridized to 5′ or 3′ UTRs (Figure 1A). The stall sites that induce NGD are located at a distance from the start codon sufficient to stall multiple ribosomes, at least 105 nt from the AUG as demonstrated in a previous study (54).

To determine if some of the tested PS-MOE ASOs reduced mRNA levels via the NGD pathway, levels of PELO and HBS1L, proteins required for NGD (48,56), were reduced in Hela cells by siRNA treatment (Figure 3A). Reduction of these NGD pathway proteins significantly decreased the activities of ASOs 1199595, 1199600, 1199616 and 1199607 as compared with activities in cells with normal levels of PELO and HBS1L, whereas activities of ASOs 1199624, 1199626 and 1199628 did not differ (Figure 3B-E and Supplementary Figure S4A, B). These experiments suggest that ASOs 1199595, 1199600, 1199616, and 1199607 may stall translation, triggering NGD; in contrast ASOs 1199624, 1199626 and 1199628, which were shown to cause alternative splicing of the *NCL* mRNA may trigger NMD.

Next, NMD factors UPF1 and SMG6 were reduced by siRNA treatment (Figure 3F). As expected, reduction of the NMD factors significantly increased the levels of *SMG5* and *ATF4* mRNAs (Supplementary Figure S4C), which are known NMD targets (64), indicating that the NMD pathway was impaired under these conditions. There was no difference in the activities of ASOs 1199595, 1199600, and 1199607 in cells depleted of UPF1 and SMG6 (Figure 3G and H and Supplementary Figure S4D). The results together suggest that these ASOs reduce the level of *NCL* mRNA mainly through the NGD pathway and not the NMD pathway. However, the activity of ASO 1199616 was decreased in cells depleted of NGD (Figure 3D) and NMD (Figure 3I) factors, suggesting that this ASO may induce mRNA decay through both pathways. The dramatically decreased activities of ASOs 1199626 (Supplementary Figure S4E) and 1199628 (Figure 3J) upon reduction of UPF1 and SMG6 indicate that these ASOs trigger the NMD pathway to reduce *NCL* mRNA levels.

To confirm that the activities of these uniform PS-MOE ASOs do not require RNase H1, RNase H1 protein was reduced by siRNA treatment in HeLa cells (Figure 3K). Reduction of RNase H1 did not affect the activities of ASOs acting via either NGD or NMD pathways (Figure 3L and Supplementary Figure S4F). The activity of an RNase H1-dependent gapmer ASO 395254 was dramatically reduced under this condition (Supplementary Figure S4G). Importantly, the activity of another gapmer ASO, which targets the same site as the ASO 1199600, was also decreased by RNase H1 reduction, and not by reduction of NGD factors (Supplementary Figure S4H). That the PS-MOE ASOs do not trigger RNase H1 cleavage but rather trigger mRNA decay is further supported by the observation that the active decay-triggering ASOs and the RNase H1-dependent 5–10-5 gapmer ASOs bind to different regions of *NCL* (Supplementary Figure S5). These observations also infer that the accessibility of the target site, as evidenced by the active sites found for gapmer ASOs, is not sufficient for uniform PS-MOE ASOs to trigger mRNA decay.

Activities of PS-MOE ASOs are translation-dependent and these ASOs can inhibit translation

The NGD pathway requires ribosome stalling on translating mRNAs (48). Therefore, if the PS-MOE ASO triggers NGD, ASO activity should also be translation dependent. To evaluate this, translation was inhibited by cycloheximide (CHX) treatment. HeLa cells were transfected with ASOs 1199600, 1199607, 1199616 or 1199628 in the presence or absence of CHX. Control cells were treated with CHX alone. In the presence of CHX, the activities of all tested ASOs were inhibited, including the PELO/HBS1L-dependent ASOs 1199600, 1199607, 1199616 and the UPF1/SMG6-dependent ASO 1199628 (Figure 4A-D). The graduate reduction of the NCL mRNA during CHX treatment was most likely due to cytotoxic effects of the drug. The loss of UPF1/SMG6-dependent ASO activity is consistent with the previous report that NMD is translation dependent (44).

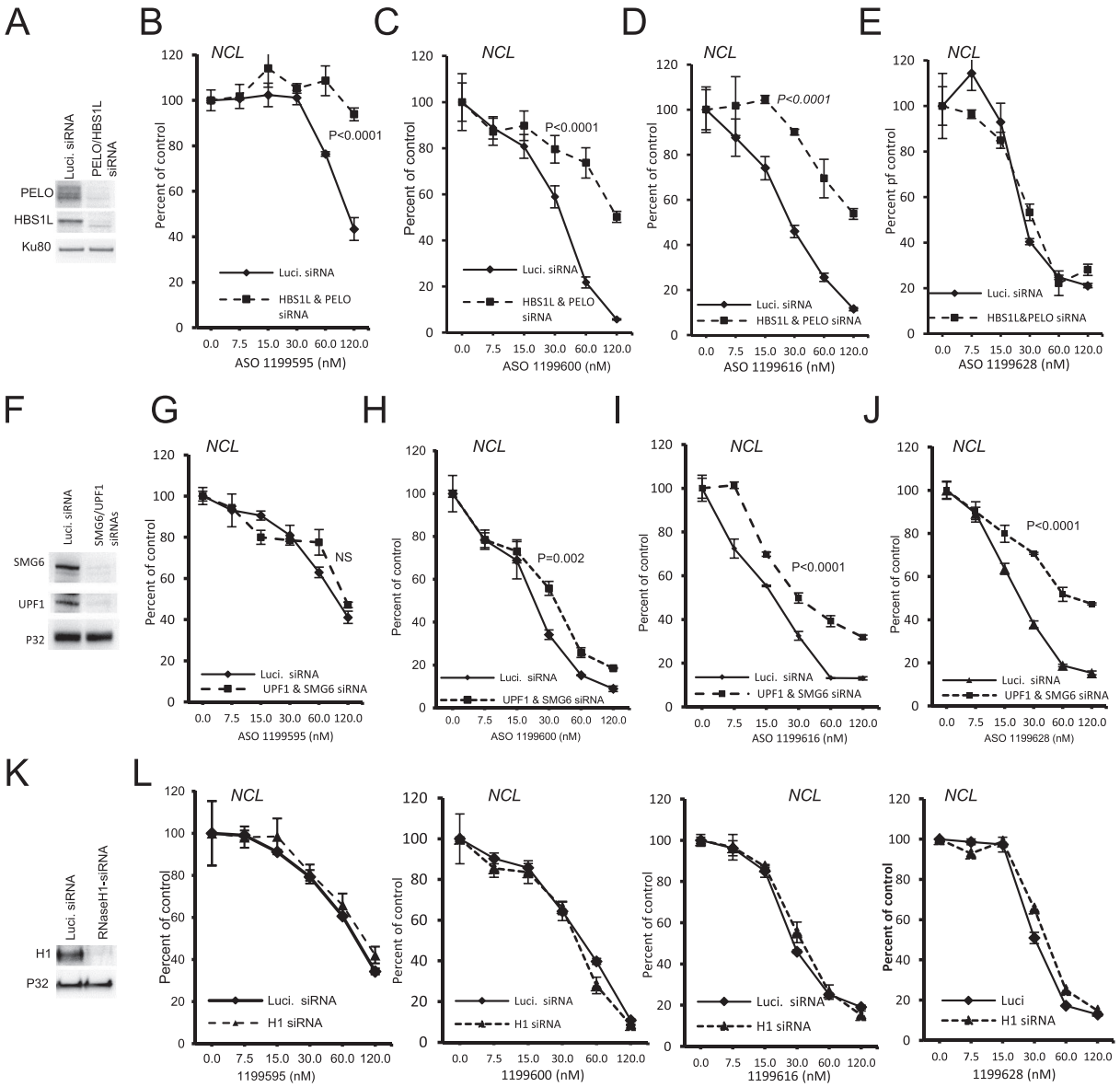

Figure 3. Certain PS-MOE ASOs reduce levels of *NCL* mRNA by inducing NGD. (**A**) Western analyses for the levels of PELO and HBS1L in HeLa cells 72 h after transfection with control *luciferase*-targeted siRNA (luci-siRNA) or siRNAs specific for *PELO* and *HBS1L*. Ku80 protein served as a control for loading. (**B–E**) qRT-PCR quantification of the levels of *NCL* mRNA in control or PELO/HBS1L-depleted HeLa cells at 18 h after ASO transfection. (**F**) Western analyses of the levels of SMG6 and UPF1 proteins in HeLa cells 72 h after transfection with luci-siRNA or siRNAs specific for *SMG6* and *UPF1*. P32 protein served as a control for loading. (**G–J**) qRT-PCR quantification of the levels of *NCL* mRNA in control or SMG6/UPF1-depleted HeLa cells 18 h after transfection with ASO. (**K**) Western analyses for the levels of RNase H1 in HeLa cells 72 h after transfection with luci-siRNA or siRNAs specific for *RNase H1* mRNA. P32 protein served as a control for loading. (**L**) qRT-PCR quantification for the levels of *NCL* mRNA in control or RNase H1-depleted HeLa cells 18 h after transfection with ASO. Error bars represent standard deviations from three independent experiments. *P*-values were calculated with *F*-test using Prism. NS, not significant.

The NGD pathway is triggered by ribosomes stalled on mRNA due to obstacles such as stable mRNA structure (49). It is therefore possible that the PELO/HBS1L-dependent ASOs base pair with the target mRNA and block ribosome scanning, leading to ribosome stalling on the mRNA. To test this possibility, HeLa cells were transfected with ASO 1199600, and the polysome profile was analyzed after 16 hour by sucrose gradient fractionation. As expected, ASO treatment reduced the level of *NCL* mRNA in cells (Figure 4E). After gradient fractionation, the levels of *NCL* mRNA in each fraction were quantified using qRT-PCR and normalized to the levels of an untargeted mRNA, *ANXA2*, in the same fractions. The *NCL* mRNA levels were modestly increased in lighter polysome fractions (F16–F20), whereas the mRNA levels in heavier polysome fractions (e.g. F24–F26) were reduced as compared with that in mock-treated control cells (Figure 4F).

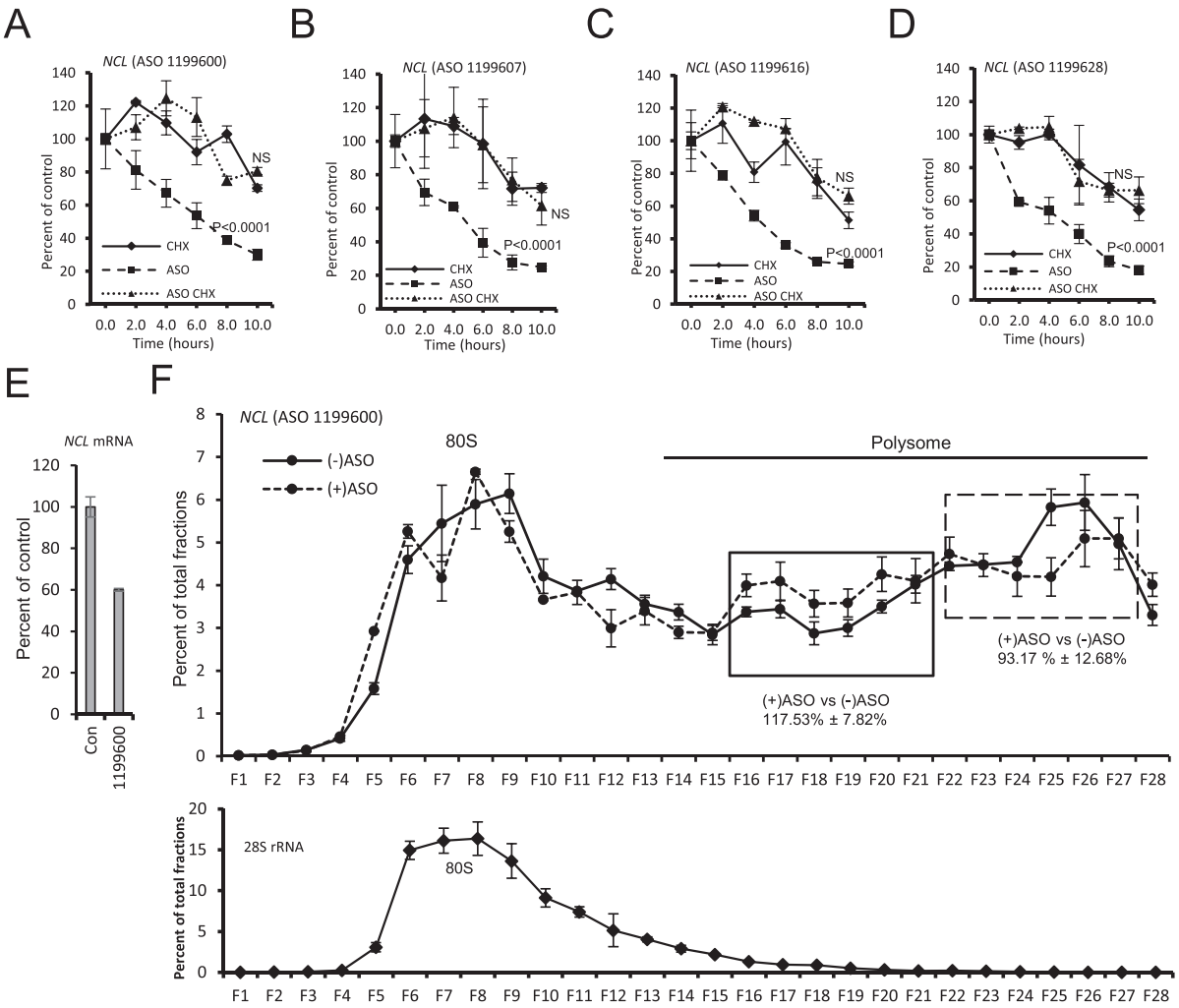

Figure 4. The activities of PS-MOE ASOs are translation dependent. (**A–D**) qRT-PCR quantification of the levels of *NCL* mRNA in HeLa cells treated for different times with ASO alone, ASO and 100 μg/ml CHX (ASO CHX), or 100 μg/ml CHX alone. The ASOs used are indicated in each panel. *P*-values were calculated with *F*-test using Prism. NS, not significant. (**E**) qRT-PCR quantification of the levels of *NCL* mRNA in Hela cells treated with or without ASO 1199600 for 16 h. (F) qRT-PCR quantification of *NCL* mRNA levels in each fraction of sucrose gradients. The amount of *NCL* mRNA in each fraction relative to the total mRNA in all fractions was calculated, as described in Materials and Methods section. The 80S monosome and polysome fractions were detected by qRT-PCR using primer probe sets specific for 28S rRNA (lower panel). The fractions with significantly different *NCL* mRNA polysome profiles with and without ASO are boxed, with solid box indicates increased levels whereas dashed box indicates reduced levels in the polysomes upon ASO treatment. The average level changes and standard deviations in those fractions are shown.

Similar results were observed when polysome profiles were analyzed 24 h after transfection (Supplementary Figure S6A) and when cells were transfected with another PS-MOE ASO 1199595, which has PELO/HBS1L-dependent activity (Supplementary Figure S6B). Though the changes in the polysome profile were modest likely due to degradation of the mRNAs bound by stalled ribosomes, the trend was highly reproducible. These observations suggest that these PS-MOE ASOs impaired the translation process as heavier polysomes shifted towards lighter polysomes in the ASO-treated compared to mock-treated cells. The levels of *NCL* mRNAs in 80S mono-ribosomes were not affected by ASO treatment, suggesting that translation initiation was not blocked. This is consistent with the fact that the ASO binding sites are downstream of the start codon. The PS-MOE ASO 1199628, which is UPF1/SMG6-dependent and most likely acts on pre-mRNA and not on mature mRNA, did not substantially affect the polysome profile of *NCL* mRNA (Supplementary Figure S6C), although this ASO also reduced the level of *NCL* mRNA in cells, supporting our hypothesis that PS-MOE ASO can act through different mechanisms to trigger mRNA decay.

La mRNA can be reduced by PS-MOE ASOs

Next, we tested whether PS-MOE ASOs can reduce the levels of other mRNAs via the NGD pathway. We designed 44 20-mer uniform PS-MOE ASOs to target various regions of *La* mRNA (Figure 5A). These ASOs were transfected into HeLa cells, and *La* mRNA levels were quantified using qRT-PCR. Some ASOs, primarily targeting the 3′ part of the coding region and >300 nt downstream from the start

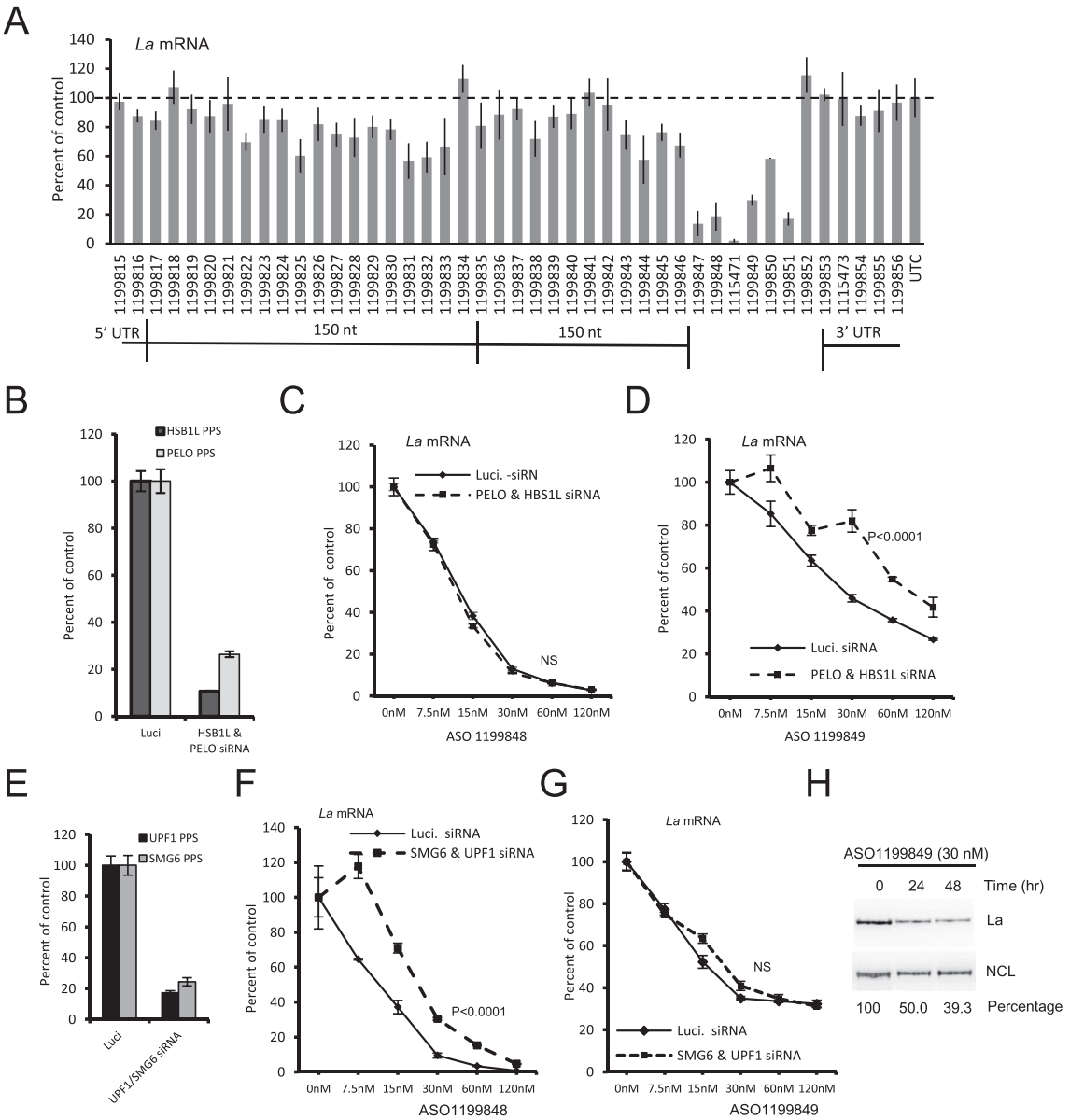

Figure 5. *La* mRNA can also be marked for NGD by PS-MOE ASOs. (**A**) qRT-PCR quantification of the levels of *La* mRNA in HeLa cells at 18 h after transfection with 120 nM ASOs. The positions of ASO target sites relative to the AUG start codon of *La* mRNA are indicated. (**B**) qRT-PCR quantifications of the levels of *PELO* and *HBS1L* mRNAs in HeLa cells 72 h after transfection with luci-siRNA or siRNAs specific for *PELO* and *HBS1L*. (**C**, **D**) qRT-PCR quantification of the levels of *La* mRNA in control or PELO/HBS1L-depleted cells 18 h after transfection with ASOs. (**E**) qRT-PCR quantification of the levels of *UPF1* and *SMG6* mRNAs in HeLa cells at 72 h after transfection with luci-siRNA or siRNAs specific for *UPF1* and *SMG6*. (**F**–**G**) qRT-PCR of *La* mRNAs in control or SMG6/UPF1-depleted cells 18 h after transfection with ASOs. Error bars are standard deviations from three independent experiments. *P*-values were calculated with *F*-test using Prism. NS, not significant. (**H**) Western analyses of the level of La protein in HeLa cells treated with 60 nM ASO1199849 for different times. The relative levels of La protein were quantified using ImageJ, normalized to the levels of NCL protein.

codon, significantly reduced the levels of *La* mRNA. No obvious mRNA reduction was observed for ASOs targeting either the 5′ or the 3′ UTR.

In cells depleted of PELO and HBS1L (Figure 5B), the activity of ASO 1199848 was not altered compared to cells treated with a control siRNA (Figure 5C), but the activity of ASO 1199849 was reduced significantly (Figure 5D), suggesting that certain PS-MOE ASOs decrease the level of *La* mRNA via the NGD pathway. Reduction of UPF1 and SMG6 decreased the activity of ASO 1199848 but not the activity of ASO 1199849 (Figure 5E–G), indicative of degradation mediated by the NMD pathway for ASO 1199848. As expected, treatment by ASO 1199849 reduced the level of La protein (Figure 5H). In addition, ASO 1199849 treatment also modestly altered polysome profile, with slightly increased *La* mRNA levels in lighter polysome fractions and reduced levels in heavier polysome fractions (Supplementary Figure S7), similar to what we observed with the NGD ASOs targeting *NCL* mRNA (Figure 4F and Supplementary Figure S6A-B). Together, these results

indicate that ASO-induced NGD is not restricted to *NCL* mRNA.

NGD triggered by ASO binding is mediated by base pairing with mRNA

As described above, the effects of PS-MOE ASOs on the levels of *NCL* mRNA are dependent on the position of the ASO binding site within the mRNA, suggesting that the ASOs act through base pairing with the target transcript. To confirm this, we evaluated ASOs of different lengths under the assumption that shorter ASO will have reduced affinity for the mRNA and should be less likely to inhibit ribosome scanning. ASOs shorter by 2 or 4 nt from either the 5′ or the 3′ end of ASO 1199600 were transfected into HeLa cells and activity evaluated (Figure 6A, upper panel). The shorter ASOs were not as active as ASO 1199600 (Figure 6A, lower panel). The 16-mer ASO (1288686) that lacks 4 nt from the 5′ end of ASO 1199600 was much less active, whereas the other 16-mer ASO (1288688) shortened from the 3′ end had reduced activity but to a lesser extent. The difference can be explained by the G-C contents of these ASOs. ASO 1288686 lacks three C-G pairs relative to ASO 1199600, whereas 1288688 lacks only one C–G pair.

The mRNA binding affinities for these ASOs were measured by analysis of thermal melting curves. The T_ms of ASO 1288686 and ASO 1288688 with an oligoribonucleotide target were reduced by 8.9°C and 5.3°C, respectively, compared with the duplex formed by the parental ASO 1199600 (Figure 6A, upper table), suggesting that ASOs with lower T_m are less able to block ribosome translocation. Shorter versions of ASO 1199616 also had reduced activity, and, as observed for the ASO 1199600 series of ASOs, the T_ms of the shorter ASOs were substantially lower than those of the parental ASO (Figure 6B).

To confirm that the decreased activities of the 16-mer ASOs were due to weaker base-pairing interactions with the target mRNA, rather than ASO length, 20-mer PS-MOE ASOs were designed that contain 2, 4, or 6 mismatches as compared with ASO 1199600. The mismatched ASOs did not as effectively decrease levels of *NCL* mRNA as did ASO 1199600, and the least active ASO was the one with six mismatches to the target (Figure 6C). Similar trends were observed with another ASO sequence, 1199616, with increasing mismatches from 5′ end further reduced the ASO activity (Figure 6D). In addition, 1, 2 or 3 mismatches were introduced into the central region of ASO 1199600 or 1199616. Consistently, central mismatches also reduced ASO activity, and more mismatches led to greater reduction in activity (Figure 6E, F). These results together suggest that the ASOs require base-pairing with target RNAs, and that the binding affinity is important for the ASOs that induce NGD. High T_m might be required to efficiently stall ribosomes.

The activities of ASOs triggering NGD pathway can be affected by chemical modifications

It is known that chemical modifications significantly affect ASO binding affinity to RNA targets. Compared with MOE modification, which can increase T_m by 0.5–1°C per modification, cEt increases T_m by 2–5°C per modification (21–23). To determine whether cEt modified ASOs exhibit greater activity than MOE-modified ASOs, we tested ASOs with three, four, or five cEt-modified nucleotides at either 5′ or 3′ end of ASOs of the same sequence as ASO 1199600. These ASOs were also modified with PS and with 2′-MOE at the non-cEt positions. These cEt-containing ASOs had higher T_ms (>90°C, data not shown) than the PS-MOE parent, but, unexpectedly, all the cEt-containing ASOs were less effective at reducing *NCL* mRNA levels than PS-MOE ASO 1199600 (Figure 7A).

Similar results were also observed for the ASO 1199616 sequence: ASOs with three, four, or five cEt modified nucleotides at either end of the ASO did not reduce *NCL* mRNA levels to the extent that the parent PS-MOE ASO did (Figure 7B). Although the exact mechanism underlying this observation is unclear, it is possible that multiple cEt-containing ASOs may have stronger self-assembly, or more tightly bind to cellular proteins, which may reduce the ASO availability for RNA binding or inhibit the functions of proteins involved. It was demonstrated previously that 2′ modifications significantly alter the binding of ASOs to cellular proteins, which can in turn affect ASO activity via different mechanisms (13,24,65,66). PS-ASOs with cEt modifications bind proteins more tightly and more avidly than do of PS-MOE ASOs (20,27).

Chemical modifications can affect ASO-protein interaction that may influence ASO activity

To determine whether the cEt-containing ASOs mediating the NGD pathway also bind more proteins than the PS-MOE ASOs, affinity selection was performed using a biotinylated PS-ASO, and bound proteins were eluted by competition using a PS-MOE ASO 1199616 or cEt-containing ASOs (1215826 and 1215829) of the same sequence, as described previously (26). Consistent with our previous observations for other proteins (27), more PELO and HBS1L was isolated with the cEt-modified ASOs than that with the PS-MOE ASO, as determined by western analyses (Figure 7C). Similarly, several other tested proteins, including hnRNP K, hnRNP A1 and NMD factors UPF1 and SMG6, also showed tighter binding to the cEt-containing ASOs. As expected, Ku80, which is less affected by 2′-modifications than many other proteins (27), bound similarly to these ASOs. Sar1b, a COPII protein that does not bind PS-ASOs (67), was not co-isolated.

That the cEt-modified ASOs bound more tightly to HBS1L than the PS-MOE parent was also confirmed with a different ASO sequence using a sensitive, bioluminescence resonance energy transfer (BRET) assay (20). In this assay, the protein of interest was fused with Nanoluc luciferase, which serves as a donor to transfer light energy to Alex 594-linked ASO when they bind. Compared with the PS-MOE ASO, cEt-modified ASOs exhibited 3–5-fold higher binding affinities (Figure 7D).

We note that the binding of PELO/HBS1L to ASOs is most likely mediated by the PS-backbone modification, and not by the ASO sequence or base-pairing with *NCL* mRNA, as different PS-MOE ASOs targeting a nucleolar snoRNA also bound these two proteins (Supplementary Figure S8). In addition, a PS-MOE modified

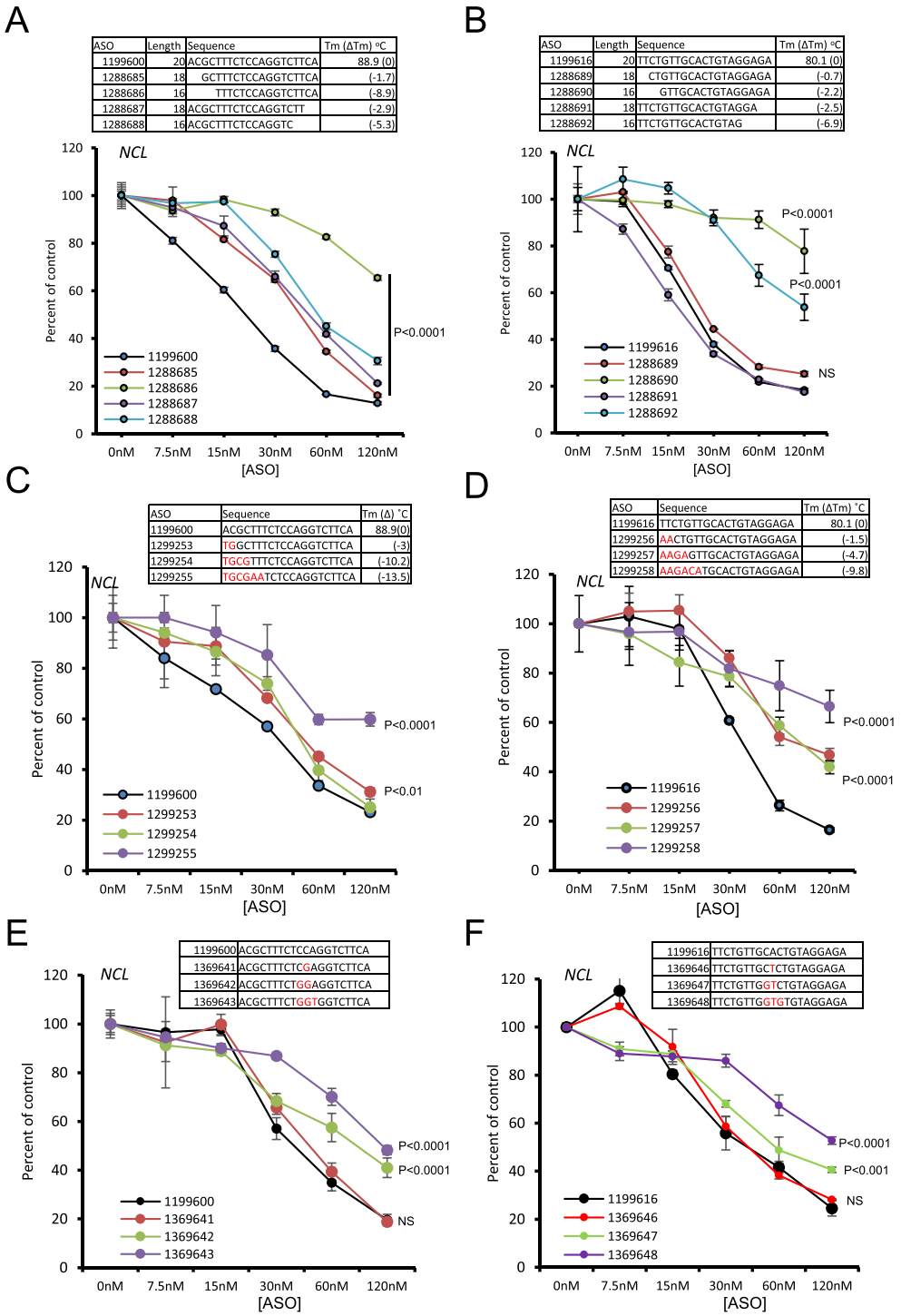

Figure 6. Efficiency of NGD of targeted mRNA depends on ASO-RNA base-pairing. (**A**) qRT-PCR quantification of the levels of *NCL* mRNA in HeLa cells 18 h after transfection with PS-MOE ASO derivatives of ASO 1199600 of different lengths. The sequences of ASOs and ΔT_m values (difference as compared with that of the parental ASO) are shown in the table. (**B**) qRT-PCR quantification of the levels of *NCL* mRNA in HeLa cells 18 h after transfection with PS-MOE ASO derivatives of ASO 1199616. The sequences of ASOs and ΔT_m values are shown in the table. (**C**) qRT-PCR quantification of the levels of *NCL* mRNA in HeLa cells 18 h after transfection with PS-MOE ASOs containing different mismatches at 5′ end of ASO 1199600. The sequences of ASOs and ΔT_m values are shown in the table. The mismatched sequences are shown in red. (**D**) qRT-PCR quantification of the levels of *NCL* mRNA in HeLa cells 18 h after transfection with PS-MOE ASOs containing different mismatches at 5′ end of ASO 1199616. The sequences of ASOs and ΔT_m values are shown in the table. The mismatched sequences are shown in red. (**E**) qRT-PCR quantification of the levels of *NCL* mRNA in HeLa cells 18 h after transfection with PS-MOE ASOs containing different central mismatches of ASO 1199600. The mismatched sequences are shown in red. (**F**) qRT-PCR quantification of the levels of *NCL* mRNA in HeLa cells 18 h after transfection with PS-MOE ASOs containing different central mismatches of ASO 1199616. The mismatched sequences are shown in red. Error bars are standard deviations from three independent experiments. *P*-values were calculated with *F*-test using Prism. NS, not significant.

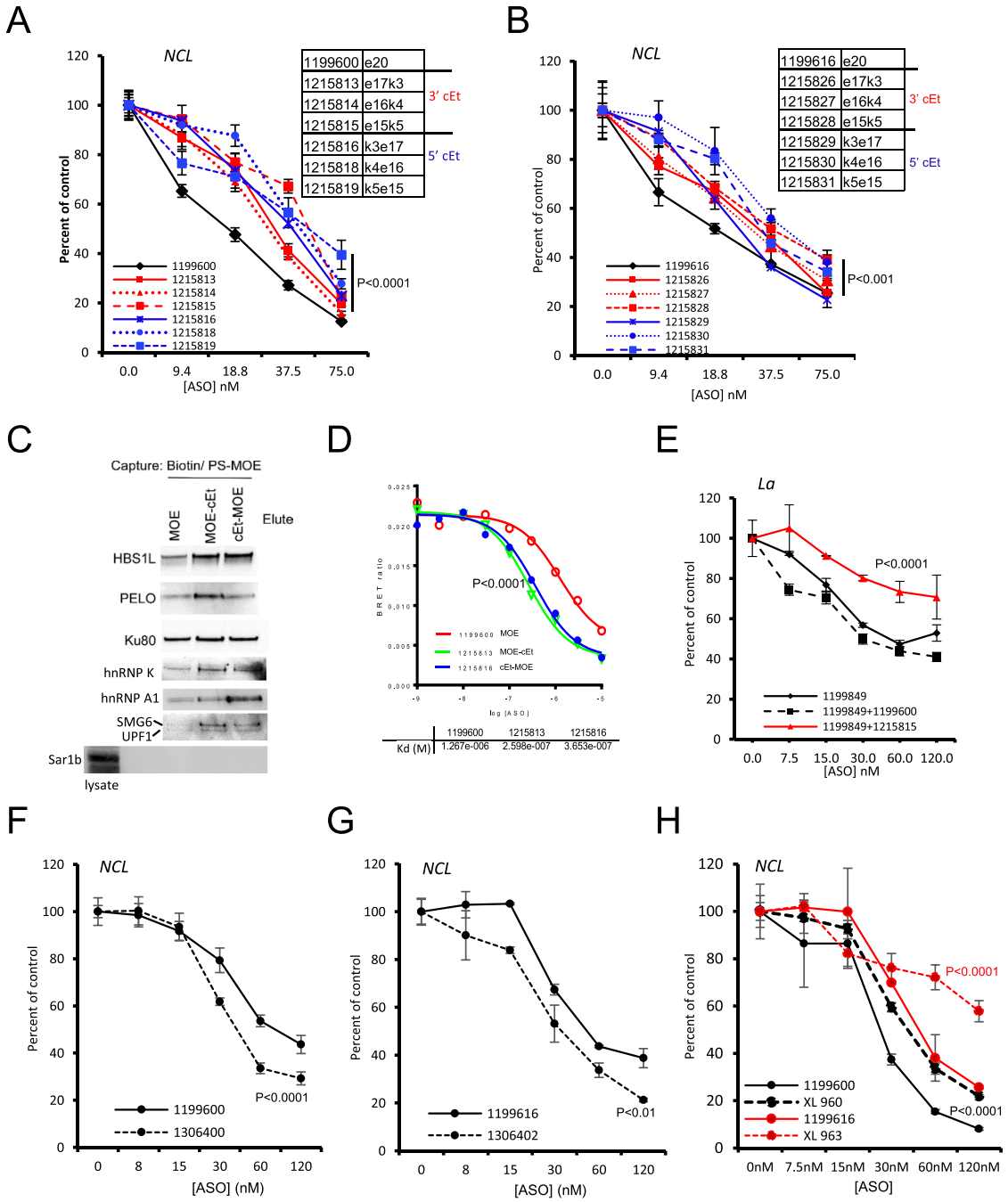

Figure 7. Chemical modification can affect the activity of ASOs inducing NGD. (**A**) qRT-PCR quantification of the levels of *NCL* mRNA in HeLa cells 18 h after transfection with ASOs that have the same sequence as ASO 1199600 but with different 2′ modification as indicated in the table. 'e' indicates a MOE modification, whereas 'k' indicates a cEt modification. (**B**) qRT-PCR quantification of the levels of *NCL* mRNA in HeLa cells 18 h after transfection with ASOs that have the same sequence as ASO 1199616 but different 2′ modification as indicated in the table. (**C**) Western analyses of NGD and NMD proteins isolated by affinity selection with 20-mer PS-MOE ASO 1199616 or cEt-containing ASOs 1215826 and 1215829. A known PS-ASO binding protein Ku80, and a known protein (Sar1b) that does not bind PS-ASO were probed to control for the quality of affinity selection. (**D**) BRET-assay of the interaction between HBS1L and indicated ASOs. The k_d values were calculated using Prism. (**E**) qRT-PCR quantification of the levels of *La* mRNA in HeLa cells 18 h after transfection with ASOs with or without 50 nM competitor: PS-MOE ASO 1199600 or cEt-containing ASO 1215815. (**F**) qRT-PCR quantification of the levels of *NCL* mRNA in HeLa cells 18 h after transfection with PS-MOE ASO 1199600 or with the one-cEt containing PS-MOE ASO 1306400 that has the same sequence as 1199600. (**G**) qRT-PCR quantification of the levels of *NCL* mRNA in HeLa cells 18 h after transfection with PS-MOE ASO 1199616 or with the one-cEt containing PS-MOE ASO 1306402 that has the same sequence as 1199616. (**H**) qRT-PCR quantification of the levels of *NCL* mRNA in HeLa cells 18 h after transfection with PS-MOE ASOs (1199600, 1199616) or their 2′-OMe-modified counterparts (XL960, XL963, respectively). Error bars are standard deviations from three independent experiments. *P*-values were calculated with *F*-test using Prism.

ASO targeting *NCL* mRNA (1107253) that did not reduce *NCL* mRNA levels (Figure 1A) also bound PELO/HBS1L proteins. However, conversion of this NCL ASO from PS to phosphodiester (PO) backbone resulted in loss of PELO/HBS1L binding. Together, these results indicate that PELO/HBS1L binding to ASOs is not mediated by ASO sequence or RNA targets, but is primarily mediated by the PS backbone modification, consistent with our previous observations (20,27).

The above results suggest that in addition to the ASO/mRNA interaction, other factors, such as ASO-protein interactions, may also contribute to the activities of ASOs that induce mRNA decay. It is possible that, though cEt-modified ASOs bound more tightly to the RNA target than did the PS-MOE ASO of the same sequence, the cEt-modified ASOs may also have increased binding to cellular proteins including the proteins important for NGD pathway. These ASO-protein interactions may alter or inhibit the functions of the proteins, as we recently demonstrated for 2′-F-modified ASOs that trigger degradation of certain paraspeckle proteins (28).

To test this possibility, the *La*-targeted ASO 1199849 was transfected into HeLa cells with or without different competitor ASOs targeting *NCL* mRNA (PS-MOE ASO 1199600 or cEt-containing ASO 1215815). Co-transfection of the cEt-containing ASO, but not the PS-MOE ASO, reduced the activity of the *La* ASO 1199849 (Figure 7E), raising a possibility that the cEt-modified ASO may inhibit the functions of some limiting proteins involved in the NGD activity. However, over-expression of PELO and HBS1L alone (Supplementary Figure S9A–F) or together (Supplementary Figure S9G–S9I) did not increase the activities of ASOs, suggesting that PELO/HBS1L proteins are required but not sufficient for ASO-induced NGD of targeted mRNA.

To simplify the situation, a single cEt modification was used to replace the MOE modification at the 5′ end of ASOs 1199600 and 1199616, as reducing the number of cEt modifications reduces protein binding (27). As expected, a single cEt replacement did not significantly increase protein binding as compared with the parental PS-MOE ASO, as determined by affinity selection followed by silver staining and western analyses (Supplementary Figure S10A and B). However, these single cEt-containing ASOs showed modest, but statistically significant increase in activity as compared with their parental PS-MOE ASOs (Figure 7F and G), suggesting that increasing ASO binding affinity to RNA can increase the ASO activity. To further confirm this observation, PS-ASOs uniformly modified with 2′-O-Methyl (Me) were synthesized for 1199600 and 1199616 sequences. These PS-Me ASOs showed reduced T_m (by 9.2°C and 3.5°C, respectively), as compared to their PS-MOE counterparts (with T_m at 88.9 and 80.1°C, respectively). Interestingly, reduced activities were observed for these PS-Me ASOs, as compared with the PS-MOE ASOs (Figure 7H). Altogether, these results suggest that chemical modifications can affect ASO activity, and that increasing ASO-RNA binding affinity can enhance ASO activity.

DISCUSSION

Enzyme-mediated antisense mechanisms, such as those involving RNase H1 and RISC, are widely used to modulate gene expression for both research and therapeutic purposes. ASO-mediated mechanisms that do not require a RNase enzyme have also been shown to alter RNA or protein levels by modulating pre-mRNA splicing, NMD, or mRNA translation. In this study, we found that ASOs uniformly modified with phosphorothioate and 2′-MOE, which cannot mediate cleavage of target RNA by RNase H1, can induce mRNA degradation through the no-go decay pathway. This study both describes a new approach for reducing gene expression and offers an explanation for previous observations that some RNase H1-independent ASOs reduce mRNA levels.

We designed PS-MOE ASOs to target different regions of the *NCL* mature mRNA. A subset of the ASOs evaluated reduced the levels of the mRNA. Some of these ASOs triggered alternative splicing. This is not surprising, as RNase H1-independent ASOs have been shown to modulate splicing by inhibiting binding of splicing factors to pre-mRNAs (6,7,68). The alternative splicing induced by the PS-MOE ASOs resulted in isoforms with premature termination codons and were likely degraded via the NMD pathway. We showed that the activities of the ASOs shown to influence splicing were dependent on UPF1 and SMG6, proteins required for NMD pathway.

Other of the ASOs that reduced *NCL* levels did not appear to affect splicing; these included ASO 1199595 and ASO 1199600. These ASOs caused mRNA reduction at a rate slower than ASOs that induced RNase H1 cleavage but similar to the rate of ASO-induced NMD, suggesting that these ASOs reduce the mRNA level via a decay mechanism. We discovered that the activities of ASO 1199595 and ASO 1199600 depend on PELO and HBS1L, proteins required for NGD, but not on NMD factors UPF1 and SMG6. Further supporting our hypothesis that these ASOs trigger degradation through NGD are several additional observations: First, the active ASOs are complementary to sequence in the coding region at positions located at least 160 nucleotides downstream from the start codon. This is consistent with previous findings that the stall signals that induce NGD are more than 105 nucleotides downstream from the start codon; presumably this location results in stalling of multiple ribosomes (54). Second, CHX treatment, which inhibits translation, abolished the activities of the PS-MOE ASOs 1199595 and 1199600. That the ASO activity is translation dependent is consistent with previous reports that NGD is translation dependent (48,54). Third, these ASOs altered the polysome profile of the target mRNA, suggesting that the ASOs act on mature, actively translated mRNA. Together, these results indicate that some PS-MOE ASOs can reduce mRNA levels by triggering NGD.

Interestingly, the activity of ASO 1199616 seems to be dependent on both NMD and NGD pathways. Reduction of either PELO/HBS1L or UPF1/SMG6 proteins decreased the ASO activity, suggesting that this ASO may trigger two different decay mechanisms. Unlike ASOs 1199595 and

1199600, ASO 1199616 affected splicing, and thus it may act on pre-mRNA and induce NMD. However, this ASO may also act on mature mRNA in the cytoplasm to inhibit translation, leading to NGD. Though the relative contribution of the two decay pathways to the reduction of NCL mRNA is unclear, these observations demonstrate the complexity of ASO-induced mRNA degradation.

The effects of the NGD ASOs on target mRNA reduction appear to be dependent on complementary base pairing to the target, since reducing the ASO length or introducing mismatches decreased activity. Importantly, 16-mer ASOs shortened from either the 5′ or 3′ end relative to the active 20-mer exhibited different activities that were correlated with thermodynamic stabilities of the duplex formed with target RNA. This was expected, as a high affinity interaction may be necessary to effectively block translation. It is unclear why many other ASOs targeting the coding region of the mRNA did not trigger mRNA reduction, as all the ASOs tested had the potential to form stable duplexes with the mRNA, and many ASO target sites are accessible as determined by screening using the gapmer ASO counterparts. It is possible that other factors, such as mRNA sequence context or the codons, may also contribute to the ribosome stalling induced by the ASOs. Understanding the mechanism in detail will require further investigation.

We reasoned that we could improve the efficacy of the ASOs that induce NGD by enhancing affinity. Therefore, we synthesized ASO with 3–5 cEt modifications, which stabilize nucleic acid duplexes (22). Surprisingly, ASOs containing several cEt-modifications at either 5′ or 3′ end had reduced activity compared to the PS-MOE ASOs of the same sequence. As the cEt-modification enhances protein binding, the reduced ASO activity may be due to reduced availability of ASOs for RNA binding due to binding to cellular proteins, or impaired functions of proteins important for NGD. To support the latter possibility, the activity of the *La* NGD ASO 1199849 was reduced by the presence of a cEt-modified competitor ASO, but not by a PS-MOE competitor ASO. As the competitor ASOs have a different sequence than that of the *La* ASO, the reduced activity of the *La* ASO was not caused by competition for binding to the same mRNA site. Rather, it is possible that the cEt-modified ASO binds more tightly than the PS-MOE ASO to proteins important for NGD pathway, which may inhibit the protein function.

In support of this hypothesis, the cEt-modified ASOs bind more PELO and HBS1L proteins than the PS-MOE counterpart. This is consistent with our previous observations that cEt-modified ASOs bind more tightly and move avidly to cellular proteins than the PS-MOE ASOs do (27). However, as over-expression of PELO and HBS1L did not increase the activity of the ASOs, it is possible that these two proteins are required, but not sufficient for ASO-induced NGD. Other cellular proteins may also be required for this process that could be affected by the cEt-modified ASOs. To simplify the situation, we evaluated the effects of PS-Me modification, which reduced Tm and also reduced ASO activity, as compared with their PS-MOE modified counterparts. On the other hand, introducing a single cEt modification did not significantly increase protein binding but modestly increased ASO activity. These results further support the hypothesis that increasing ASO/RNA binding affinity can increase ASO activity. However, as chemical modifications can affect ASO binding to both RNA and cellular proteins that may be necessary for NGD activity, caution needs to be taken when introducing multiple high affinity and/or lipophilic modifications to ASOs.

NGD has been reported to occur in yeast, insects, plants and mammals (48,49,52). Identifying endogenous NGD target mRNAs, which could be facilitated by ribosome profiling through determining heavily ribosome-protected regions in mRNAs, will be important for better understanding and intervening gene expression regulation. Here we found that PS-MOE ASOs can reduce the levels of different mRNAs in several human cell lines and a mouse cell line, suggesting that this mechanism of ASO activity could be employed in different species. Although the activities of the ASOs that induce NGD act more slowly than gapmer ASOs, the maximum reduction of the target RNA seemed comparable. Use of uniformly modified ASO that cannot activate RNase H1 may have advantages for some targets and can be employed in cells with low RNase H1 levels. Establishing general rules for identification of active target sites and design of more potent NGD inducing ASOs requires further investigation. However, several factors may be considered based on current study, e.g., targeting the 3′ portion of coding region of mRNAs; using ASOs with proper length and chemistry that have higher Tm yet without causing self-structure or strong protein binding; and selecting sequences with minimum off-target potential.

In addition, our studies demonstrate the complexity of ASO-RNA interactions. In the coding region of a target mRNA, different antisense mechanisms can potentially result in loss of target RNAs. These findings provide explanations for previous observations that ASOs that cannot mediate RNase H1 cleavage sometimes result in target mRNA loss (59). Furthermore, that both NMD and NGD can contribute to target RNA reduction induced by ASO treatment demonstrates that once an ASO/RNA duplex is formed competition among various proteins for the ASO/RNA duplex can cause complex effects.

SUPPLEMENTARY DATA

Supplementary Data are available at NAR Online.

ACKNOWLEDGEMENTS

We wish to thank Michael Migawa and Huynh-Hoa Bui for ASO design, Andres Berdeja for T_m measurements, Mark Andrade for ASO synthesis, Wanda Sullivan for figure preparation and Wen Shen and Shiyu Wang for valuable discussions.

FUNDING

Internal funding from Ionis Pharmaceuticals. Funding for open access charge: Ionis Pharmaceuticals.

Conflict of interest statement. All authors are employees of Ionis Pharmaceuticals. A patent related to this study has been filed.

REFERENCES

1. Crooke,S.T., Witztum,J.L., Bennett,C.F. and Baker,B.F. (2018) RNA-targeted therapeutics. *Cell Metab.*, **27**, 714–739.
2. Filipowicz,W., Jaskiewicz,L., Kolb,F.A. and Pillai,R.S. (2005) Post-transcriptional gene silencing by siRNAs and miRNAs. *Curr. Opin. Struct. Biol.*, **15**, 331–341.
3. Dias,N. and Stein,C.A. (2002) Antisense oligonucleotides: basic concepts and mechanisms. *Mol. Cancer Ther.*, **1**, 347–355.
4. Bennett,C.F. and Swayze,E.E. (2010) RNA targeting therapeutics: molecular mechanisms of antisense oligonucleotides as a therapeutic platform. *Annu. Rev. Pharmacol. Toxicol.*, **50**, 259–293.
5. Kawasaki,H., Taira,K. and Morris,K.V. (2005) siRNA induced transcriptional gene silencing in mammalian cells. *Cell Cycle*, **4**, 442–448.
6. Hua,Y., Vickers,T.A., Baker,B.F., Bennett,C.F. and Krainer,A.R. (2007) Enhancement of SMN2 exon 7 inclusion by antisense oligonucleotides targeting the exon. *PLoS Biol.*, **5**, e73.
7. Rigo,F., Hua,Y., Chun,S.J., Prakash,T.P., Krainer,A.R. and Bennett,C.F. (2012) Synthetic oligonucleotides recruit ILF2/3 to RNA transcripts to modulate splicing. *Nat. Chem. Biol.*, **8**, 555–561.
8. Nomakuchi,T.T., Rigo,F., Aznarez,I. and Krainer,A.R. (2016) Antisense oligonucleotide-directed inhibition of nonsense-mediated mRNA decay. *Nat. Biotechnol.*, **34**, 164–166.
9. Huang,L., Low,A., Damle,S.S., Keenan,M.M., Kuntz,S., Murray,S.F., Monia,B.P. and Guo,S. (2018) Antisense suppression of the nonsense mediated decay factor Upf3b as a potential treatment for diseases caused by nonsense mutations. *Genome Biol.*, **19**, 4.
10. Ward,A.J., Norrbom,M., Chun,S., Bennett,C.F. and Rigo,F. (2014) Nonsense-mediated decay as a terminating mechanism for antisense oligonucleotides. *Nucleic Acids Res.*, **42**, 5871–5879.
11. Geary,R.S., Baker,B.F. and Crooke,S.T. (2015) Clinical and preclinical pharmacokinetics and pharmacodynamics of mipomersen (kynamro((R))): a second-generation antisense oligonucleotide inhibitor of apolipoprotein B. *Clin. Pharmacokinet.*, **54**, 133–146.
12. Goodkey,K., Aslesh,T., Maruyama,R. and Yokota,T. (2018) Nusinersen in the treatment of spinal muscular atrophy. *Methods Mol. Biol.*, **1828**, 69–76.
13. Crooke,S.T., Wang,S., Vickers,T.A., Shen,W. and Liang,X.H. (2017) Cellular uptake and trafficking of antisense oligonucleotides. *Nat. Biotechnol.*, **35**, 230–237.
14. Crooke,S.T.V.T.A., Lima,W.F. and Wu,H.-J. (2008) In: Crooke,ST (ed). *Antisense Drug Technology - Principles, Strategies, and Applications*. 2nd edn. CRC Press, Boca Raton, pp. 3–46.
15. Kurreck,J. (2003) Antisense technologies. Improvement through novel chemical modifications. *Eur. J. Biochem.*, **270**, 1628–1644.
16. Bennett,C.F., Baker,B.F., Pham,N., Swayze,E. and Geary,R.S. (2017) Pharmacology of antisense drugs. *Annu. Rev. Pharmacol. Toxicol.*, **57**, 81–105.
17. Swayze,E.E. and Bhat,B. (2008) In: Crooke,ST (ed). *Antisense Drug Technology - Principles, Strategies, and Applications*. 2nd edn. CRC Press, Boca Raton, pp. 143–182.
18. Eckstein,F. (2000) Phosphorothioate oligodeoxynucleotides: what is their origin and what is unique about them? *Antisense Nucleic Acid Drug Dev.*, **10**, 117–121.
19. Agrawal,S. (1999) Importance of nucleotide sequence and chemical modifications of antisense oligonucleotides. *Biochim. Biophys. Acta*, **1489**, 53–68.
20. Vickers,T.A. and Crooke,S.T. (2016) Development of a quantitative BRET affinity assay for nucleic acid-protein interactions. *PLoS One*, **11**, e0161930.
21. Freier,S.M. and Altmann,K.H. (1997) The ups and downs of nucleic acid duplex stability: structure-stability studies on chemically-modified DNA:RNA duplexes. *Nucleic Acids Res.*, **25**, 4429–4443.
22. Seth,P.P., Vasquez,G., Allerson,C.A., Berdeja,A., Gaus,H., Kinberger,G.A., Prakash,T.P., Migawa,M.T., Bhat,B. and Swayze,E.E. (2010) Synthesis and biophysical evaluation of 2′,4′-constrained 2′O-methoxyethyl and 2′,4′-constrained 2′O-ethyl nucleic acid analogues. *J. Org. Chem.*, **75**, 1569–1581.
23. Monia,B.P., Johnston,J.F., Sasmor,H. and Cummins,L.L. (1996) Nuclease resistance and antisense activity of modified oligonucleotides targeted to Ha-ras. *J. Biol. Chem.*, **271**, 14533–14540.
24. Liang,X.H., Sun,H., Shen,W. and Crooke,S.T. (2015) Identification and characterization of intracellular proteins that bind oligonucleotides with phosphorothioate linkages. *Nucleic Acids Res.*, **43**, 2927–2945.
25. Shen,W., Liang,X.H. and Crooke,S.T. (2014) Phosphorothioate oligonucleotides can displace NEAT1 RNA and form nuclear paraspeckle-like structures. *Nucleic Acids Res.*, **42**, 8648–8662.
26. Liang,X.H., Shen,W., Sun,H., Prakash,T.P. and Crooke,S.T. (2014) TCP1 complex proteins interact with phosphorothioate oligonucleotides and can co-localize in oligonucleotide-induced nuclear bodies in mammalian cells. *Nucleic Acids Res.*, **42**, 7819–7832.
27. Liang,X.H., Shen,W., Sun,H., Kinberger,G.A., Prakash,T.P., Nichols,J.G. and Crooke,S.T. (2016) Hsp90 protein interacts with phosphorothioate oligonucleotides containing hydrophobic 2′-modifications and enhances antisense activity. *Nucleic Acids Res.*, **44**, 3892–3907.
28. Shen,W., Liang,X.H., Sun,H. and Crooke,S.T. (2015) 2′-Fluoro-modified phosphorothioate oligonucleotide can cause rapid degradation of P54nrb and PSF. *Nucleic Acids Res.*, **43**, 4569–4578.
29. Kakiuchi-Kiyota,S., Whiteley,L.O., Ryan,A.M. and Mathialagan,N. (2016) Development of a method for profiling protein interactions with LNA-Modified antisense oligonucleotides using protein microarrays. *Nucleic Acid Ther.*, **26**, 93–101.
30. Liang,X.H., Sun,H., Nichols,J.G. and Crooke,S.T. (2017) RNase H1-dependent antisense oligonucleotides are robustly active in directing RNA cleavage in both the cytoplasm and the nucleus. *Mol. Ther.*, **25**, 2075–2092.
31. Lima,W.F., De Hoyos,C.L., Liang,X.H. and Crooke,S.T. (2016) RNA cleavage products generated by antisense oligonucleotides and siRNAs are processed by the RNA surveillance machinery. *Nucleic Acids Res.*, **44**, 3351–3363.
32. Boiziau,C., Kurfurst,R., Cazenave,C., Roig,V., Thuong,N.T. and Toulme,J.J. (1991) Inhibition of translation initiation by antisense oligonucleotides via an RNase-H independent mechanism. *Nucleic Acids Res.*, **19**, 1113–1119.
33. Liang,X-h., Shen,W., Sun,H., Migawa,M.T., Vickers,T.A. and Crooke,S.T. (2016) Translation efficiency of mRNAs is increased by antisense oligonucleotides targeting upstream open reading frames. *Nat Biotech*, **34**, 875–880.
34. Liang,X.H., Sun,H., Shen,W., Wang,S., Yao,J., Migawa,M.T., Bui,H.H., Damle,S.S., Riney,S., Graham,M.J. *et al.* (2017) Antisense oligonucleotides targeting translation inhibitory elements in 5′ UTRs can selectively increase protein levels. *Nucleic Acids Res.*, **45**, 9528–9546.
35. Rouleau,S.G., Beaudoin,J.D., Bisaillon,M. and Perreault,J.P. (2015) Small antisense oligonucleotides against G-quadruplexes: specific mRNA translational switches. *Nucleic Acids Res.*, **43**, 595–606.
36. Liang,X.H., Nichols,J.G., Sun,H. and Crooke,S.T. (2018) Translation can affect the antisense activity of RNase H1-dependent oligonucleotides targeting mRNAs. *Nucleic Acids Res.*, **46**, 293–313.
37. Chen,Y.H. and Coller,J. (2016) A universal code for mRNA stability? *Trends Genet.*, **32**, 687–688.
38. Coller,J. and Parker,R. (2004) Eukaryotic mRNA decapping. *Annu. Rev. Biochem.*, **73**, 861–890.
39. Garneau,N.L., Wilusz,J. and Wilusz,C.J. (2007) The highways and byways of mRNA decay. *Nat. Rev. Mol. Cell Biol.*, **8**, 113–126.
40. Ghosh,S. and Jacobson,A. (2010) RNA decay modulates gene expression and controls its fidelity. *Wiley Interdiscip. Rev. RNA*, **1**, 351–361.
41. Jacobson,A. (2004) Regulation of mRNA decay: decapping goes solo. *Mol. Cell*, **15**, 1–2.
42. Chen,C.Y. and Shyu,A.B. (2011) Mechanisms of deadenylation-dependent decay. *Wiley Interdiscip. Rev. RNA*, **2**, 167–183.
43. Lykke-Andersen,S. and Jensen,T.H. (2015) Nonsense-mediated mRNA decay: an intricate machinery that shapes transcriptomes. *Nat. Rev. Mol. Cell Biol.*, **16**, 665–677.
44. Conti,E. and Izaurralde,E. (2005) Nonsense-mediated mRNA decay: molecular insights and mechanistic variations across species. *Curr. Opin. Cell Biol.*, **17**, 316–325.
45. Nicholson,P. and Muhlemann,O. (2010) Cutting the nonsense: the degradation of PTC-containing mRNAs. *Biochem. Soc. Trans.*, **38**, 1615–1620.

46. Karamyshev,A.L. and Karamysheva,Z.N. (2018) Lost in Translation: Ribosome-Associated mRNA and protein quality controls. *Front. Genet.*, **9**, 431.
47. Vasudevan,S., Peltz,S.W. and Wilusz,C.J. (2002) Non-stop decay–a new mRNA surveillance pathway. *BioEssays*, **24**, 785–788.
48. Doma,M.K. and Parker,R. (2006) Endonucleolytic cleavage of eukaryotic mRNAs with stalls in translation elongation. *Nature*, **440**, 561–564.
49. Harigaya,Y. and Parker,R. (2010) No-go decay: a quality control mechanism for RNA in translation. *Wiley Interdiscip. Rev. RNA*, **1**, 132–141.
50. Horikawa,W., Endo,K., Wada,M. and Ito,K. (2016) Mutations in the G-domain of Ski7 cause specific dysfunction in non-stop decay. *Sci. Rep.*, **6**, 29295.
51. Passos,D.O., Doma,M.K., Shoemaker,C.J., Muhlrad,D., Green,R., Weissman,J., Hollien,J. and Parker,R. (2009) Analysis of Dom34 and its function in no-go decay. *Mol. Biol. Cell*, **20**, 3025–3032.
52. Saito,S., Hosoda,N. and Hoshino,S. (2013) The Hbs1-Dom34 protein complex functions in non-stop mRNA decay in mammalian cells. *J. Biol. Chem.*, **288**, 17832–17843.
53. Szadeczky-Kardoss,I., Gal,L., Auber,A., Taller,J. and Silhavy,D. (2018) The No-go decay system degrades plant mRNAs that contain a long A-stretch in the coding region. *Plant Sci*, **275**, 19–27.
54. Simms,C.L., Yan,L.L. and Zaher,H.S. (2017) Ribosome collision is critical for quality control during No-Go decay. *Mol. Cell*, **68**, 361–373.
55. Simms,C.L., Kim,K.Q., Yan,L.L., Qiu,J. and Zaher,H.S. (2018) Interactions between the mRNA and Rps3/uS3 at the entry tunnel of the ribosomal small subunit are important for no-go decay. *PLoS Genet.*, **14**, e1007818.
56. Chen,L., Muhlrad,D., Hauryliuk,V., Cheng,Z., Lim,M.K., Shyp,V., Parker,R. and Song,H. (2010) Structure of the Dom34-Hbs1 complex and implications for no-go decay. *Nat. Struct. Mol. Biol.*, **17**, 1233–1240.
57. Becker,T., Armache,J.P., Jarasch,A., Anger,A.M., Villa,E., Sieber,H., Motaal,B.A., Mielke,T., Berninghausen,O. and Beckmann,R. (2011) Structure of the no-go mRNA decay complex Dom34-Hbs1 bound to a stalled 80S ribosome. *Nat. Struct. Mol. Biol.*, **18**, 715–720.
58. Hilal,T., Yamamoto,H., Loerke,J., Burger,J., Mielke,T. and Spahn,C.M. (2016) Structural insights into ribosomal rescue by Dom34 and Hbs1 at near-atomic resolution. *Nat. Commun.*, **7**, 13521.
59. Mulders,S.A., van den Broek,W.J., Wheeler,T.M., Croes,H.J., van Kuik-Romeijn,P., de Kimpe,S.J., Furling,D., Platenburg,G.J., Gourdon,G., Thornton,C.A. *et al.* (2009) Triplet-repeat oligonucleotide-mediated reversal of RNA toxicity in myotonic dystrophy. *PNAS*, **106**, 13915–13920.
60. Bleriot,Y.V., Vadivel,S.K., Herrera,A.J., Greig,I.R., Kirby,A.J. and Sinay,P. (2004) Synthesis and acid catalyzed hydrolysis of B2,5 type conformationally constrained glucopyranosides: incorporation into a cellobiose analog. *Tetrahedron*, **60**, 6813–6828.
61. Wang,S., Allen,N., Vickers,T.A., Revenko,A.S., Sun,H., Liang,X.H. and Crooke,S.T. (2018) Cellular uptake mediated by epidermal growth factor receptor facilitates the intracellular activity of phosphorothioate-modified antisense oligonucleotides. *Nucleic Acids Res.*, **46**, 3579–3594.
62. Liang,X.H., Vickers,T.A., Guo,S. and Crooke,S.T. (2011) Efficient and specific knockdown of small non-coding RNAs in mammalian cells and in mice. *Nucleic Acids Res.*, **39**, e13.
63. Vickers,T.A., Wyatt,J.R., Burckin,T., Bennett,C.F. and Freier,S.M. (2001) Fully modified 2′ MOE oligonucleotides redirect polyadenylation. *Nucleic Acids Res.*, **29**, 1293–1299.
64. Colombo,M., Karousis,E.D., Bourquin,J., Bruggmann,R. and Muhlemann,O. (2017) Transcriptome-wide identification of NMD-targeted human mRNAs reveals extensive redundancy between SMG6- and SMG7-mediated degradation pathways. *RNA*, **23**, 189–201.
65. Wang,S., Sun,H., Tanowitz,M., Liang,X.H. and Crooke,S.T. (2016) Annexin A2 facilitates endocytic trafficking of antisense oligonucleotides. *Nucleic Acids Res.*, **44**, 7314–7330.
66. Bailey,J.K., Shen,W., Liang,X.H. and Crooke,S.T. (2017) Nucleic acid binding proteins affect the subcellular distribution of phosphorothioate antisense oligonucleotides. *Nucleic Acids Res.*, **45**, 10649–10671.
67. Liang,X.H., Sun,H., Nichols,J.G., Allen,N., Wang,S., Vickers,T.A., Shen,W., Hsu,C.W. and Crooke,S.T. (2018) COPII vesicles can affect the activity of antisense oligonucleotides by facilitating the release of oligonucleotides from endocytic pathways. *Nucleic Acids Res.*, **46**, 10225–10245.
68. Dunckley,M.G., Manoharan,M., Villiet,P., Eperon,I.C. and Dickson,G. (1998) Modification of splicing in the dystrophin gene in cultured Mdx muscle cells by antisense oligoribonucleotides. *Hum. Mol. Genet.*, **7**, 1083–1090.